# Charge radius of the short-lived $^{68}$Ni and correlation with the dipole polarizability

S. Kaufmann,$^1$ J. Simonis,$^2$ S. Bacca,$^{2,3}$ J. Billowes,$^4$ M. L. Bissell,$^4$ K. Blaum,$^5$ B. Cheal,$^6$ R. F. Garcia Ruiz,$^{4,7}$
W. Gins,$^8$ C. Gorges,$^1$ G. Hagen,$^9$ H. Heylen,$^{5,7}$ A. Kanellakopoulos,$^8$ S. Malbrunot-Ettenauer,$^7$ M. Miorelli,$^{10}$ R.
Neugart,$^{5,11}$ G. Neyens,$^{7,8}$ W. Nörtershäuser,$^{1,*}$ R. Sánchez,$^{12}$ S. Sailer,$^{13}$ A. Schwenk,$^{1,5,14}$ T. Ratajczyk,$^1$
L. V. Rodríguez,$^{15}$ L. Wehner,$^{16}$ C. Wraith,$^6$ L. Xie,$^4$ Z. Y. Xu,$^8$ X. F. Yang,$^{8,17}$ and D. T. Yordanov$^{15}$

$^1$*Institut für Kernphysik, Technische Universität Darmstadt, D-64289 Darmstadt, Germany*
$^2$*Institut für Kernphysik and PRISMA$^+$ Cluster of Excellence,*
*Johannes Gutenberg-Universität Mainz, D-55128 Mainz, Germany*
$^3$*Helmholtz-Institut Mainz, Johannes Gutenberg-Universität Mainz, D-55099 Mainz, Germany*
$^4$*School of Physics and Astronomy, The University of Manchester, Manchester, M13 9PL, United Kingdom*
$^5$*Max-Planck-Institut für Kernphysik, D-69117 Heidelberg, Germany*
$^6$*Oliver Lodge Laboratory, Oxford Street, University of Liverpool, Liverpool, L69 7ZE, United Kingdom*
$^7$*Experimental Physics Department, CERN, CH-1211 Geneva 23, Switzerland*
$^8$*KU Leuven, Instituut voor Kern- en Stralingsfysica, B-3001 Leuven, Belgium*
$^9$*Physics Division, Oak Ridge National Laboratory, Oak Ridge,*
*Tennessee 37831, USA and Department of Physics and Astronomy,*
*University of Tennessee, Knoxville, TN 37996, USA*
$^{10}$*TRIUMF, 4004 Wesbrook Mall, Vancouver, British Columbia, V6T 2A3, Canada*
$^{11}$*Institut für Kernchemie, Johannes Gutenberg-Universität Mainz, D-55128 Mainz, Germany*
$^{12}$*GSI Helmholtzzentrum für Schwerionenforschung, D-64291 Darmstadt, Germany*
$^{13}$*Technische Universität München, D-80333 München, Germany*
$^{14}$*ExtreMe Matter Institute EMMI, GSI Helmholtzzentrum für Schwerionenforschung GmbH, D-64291 Darmstadt, Germany*
$^{15}$*Institut de Physique Nucléaire, CNRS-IN2P3, Université Paris-Sud, Université Paris-Saclay, 91406 Orsay, France*
$^{16}$*Institut für Kernchemie, Universität Mainz, D-55128 Mainz, Germany*
$^{17}$*School of Physics and State Key Laboratory of Nuclear Physics and Technology, Peking University, Beijing 100871, China*

We present the first laser spectroscopic measurement of the neutron-rich nucleus $^{68}$Ni at the
$N = 40$ subshell closure and extract its nuclear charge radius. Since this is the only short-lived
isotope for which the dipole polarizability $\alpha_{\mathrm{D}}$ has been measured, the combination of these observables provides a benchmark for nuclear structure theory. We compare them to novel coupled-cluster
calculations based on different chiral two- and three-nucleon interactions, for which a strong correlation between the charge radius and dipole polarizability is observed, similar to the stable nucleus
$^{48}$Ca. Three-particle–three-hole correlations in coupled-cluster theory substantially improve the description of the experimental data, which allows to constrain the neutron radius and neutron skin
of $^{68}$Ni.

## INTRODUCTION

The nuclear equation of state (EOS) plays a key role
in supernova explosions and compact object mergers. In
fact, the gravitational wave signal from the neutron star
merger GW170817 has recently lead to constraints on
the EOS of neutron-rich matter [1], which is consistent
with our knowledge of nuclear physics. While the EOS of
symmetric nuclear matter is well constrained around saturation density [2], the properties of neutron-rich matter
are still rather uncertain. These properties are encoded
in the nuclear symmetry energy $S(n)$ as a function of
density $n$ and the slope parameter $L = 3n_0\partial S(n_0)/\partial n$
at saturation density $n_0$. Studies on atomic nuclei can
provide information on the $L$ parameter [3] through a
nuclide's neutron-skin thickness $R_{\mathrm{skin}} = R_{\mathrm{n}} - R_{\mathrm{p}}$ defined
as the difference between the point-neutron and point-
proton radii. The neutron skin is a consequence of the
competition between the surface tension and the pressure of neutron matter, which is determined by the $L$
parameter. In the heavy nucleus $^{208}$Pb energy density
functional (EDF) calculations confirmed this strong cor-

relation between $R_{\mathrm{skin}}$ and $L$ with a correlation coefficient of 0.979. This allows one to further constrain $L$
based on $R_{\mathrm{skin}}$ [4]. Unfortunately, the direct measurement of $R_{\mathrm{skin}}$ is experimentally very challenging. In recent measurements it was extracted by its correlation to
the dipole polarizability $\alpha_{\mathrm{D}}$, which can be explored, e.g.,
with proton inelastic scattering, as it was the case for
$^{48}$Ca [5], $^{120}$Sn [6] and $^{208}$Pb [7]. Here mostly EDFs were
used to extract the neutron skin from the dipole polarizability, but in the case of $^{48}$Ca the neutron skin was predicted from first principles coupled-cluster calculations
to be surprisingly small, only 0.12–0.15 fm [8]. These ab
initio calculations starting from two- and three-nucleon
interactions based on chiral effective field theory (EFT)
[9–11] further revealed a correlation between the charge
radius and the dipole polarizability, which was predicted
to be in the range 2.19–2.60 fm$^3$. Recent measurements
of $^{48}$Ca by Birkhan *et al.* [5] yielded a dipole polarizability of $\alpha_{\mathrm{D}} = 2.07(22)$ fm$^3$ in agreement with the chiral
EFT predictions. The only short-lived nucleus for which
$\alpha_{\mathrm{D}}$ has been experimentally determined is $^{68}$Ni, using
Coulomb excitation in inverse kinematics. The pygmy

and the giant dipole resonances were observed and $\alpha_\mathrm{D}$ was extracted [12]. In this Letter, we focus on the charge radius of $^{68}$Ni, determined by collinear laser spectroscopy. It is the first laser spectroscopy result on a short-lived nickel isotope, since access to this element at ISOL facilities is limited due to the slow release from the target. On the theory side, we report on the first coupled-cluster calculation including triples of $R_\mathrm{c}$ and $\alpha_\mathrm{D}$ of $^{68}$Ni based on chiral EFT interactions, being now the heaviest system for which this has been achieved. We study the correlation of the charge radius with the dipole polarizability in novel ab initio calculations including triples contributions. The measured charge radius in combination with the experimental dipole polarizability enables the first test of this correlation in a neutron-rich medium-mass nucleus.

## EXPERIMENT

Nickel isotopes were produced at ISOLDE/CERN using proton pulses at an energy of $1.4\,\mathrm{GeV}$ to cause fragmentation, spallation, and fission inside a uranium carbide target. The target was heated beyond standard operation temperatures up to $\sim 2200\,^{\circ}\mathrm{C}$ to enhance the release of chemically reactive nickel isotopes that have generally quite long release times from the target. Nickel atoms were then ionized by resonant laser ionization using RILIS [13] and accelerated towards the high-resolution mass separator on ground potential by applying an electrostatic potential of approximately $30\,\mathrm{kV}$ and $40\,\mathrm{kV}$ to the ion source in a first and a second beam-time, respectively. The mass separated ions were injected into the radio-frequency ion beam cooler and buncher IS-COOL [14] and accumulated for typically $10 - 100\,\mathrm{ms}$. Extracted ion bunches of $5\,\mu\mathrm{s}$ duration were transported to the collinear laser spectroscopy beam line COLLAPS where the ions were superimposed with a co-propagating laser beam. Potassium vapor in a charge-exchange cell [15, 16] was used to neutralize the ions. Various excited states of the nickel atoms were populated within this non-resonant process, among them the metastable $3d^9\,4s\,{}^3D_3$ level [17] that served as the starting point for laser spectroscopy, performed in the $352.45\,\mathrm{nm}$ transition to the $3d^9\,4p\,{}^3P_2$ level. Fluorescence photons from spontaneous emission were detected by four photomultiplier tubes and the individual events were recorded with a new time-resolving data acquisition system. The laser light was produced using a frequency-doubled single-mode continuous-wave titanium sapphire laser stabilized on a high-resolution wavemeter, which was calibrated regularly with a stabilized helium-neon laser. Typical spectra of the isotopes $^{58,60,61,62,64,68}$Ni are shown in Fig. 1. All isotopes were measured alternating with the reference isotope $^{60}$Ni to compensate for any remaining long-term drifts in the ion velocity or the laser frequency.
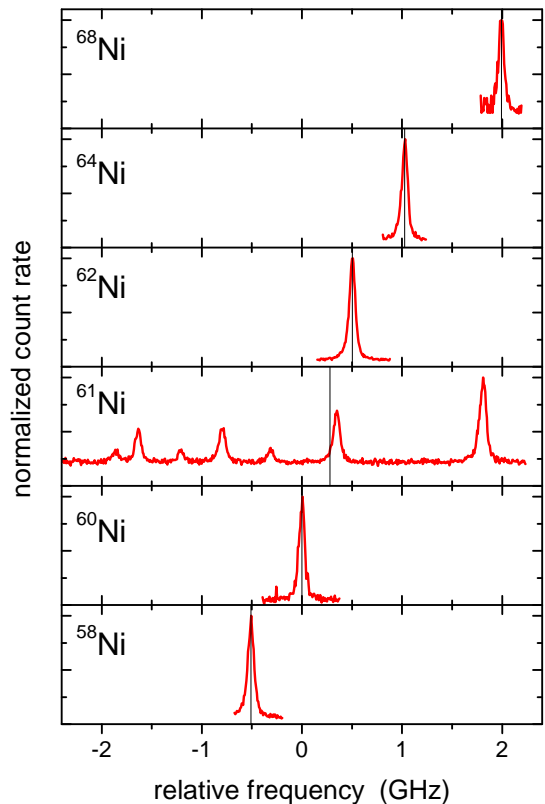


FIG. 1. Spectra of the stable isotopes $^{58,60,61,62,64}$Ni and the radioactive $^{68}$Ni with their center frequency indicated with a vertical line. The count rate is normalized for each isotope, and the frequency is given relative to the center frequency of the reference isotope $^{60}$Ni.

## ANALYSIS

Isotope shifts $\delta\nu^{60,A} = \nu^A - \nu^{60}$ for the stable isotopes $^{58,61,62,64}$Ni and the radioactive $^{68}$Ni were calculated from their respective center frequency $\nu^A$ with respect to the center frequency $\nu^{60}$ of the reference isotope $^{60}$Ni. Results are listed in Table I. Isotope shifts are related to differences in mean-square charge radii $\delta\left\langle r_\mathrm{c}^2\right\rangle^{60,A}$ via a field shift factor $F$ and a mass shift factor $M$ according to

$$\delta\nu^{60,A} = \mu \cdot M + F \cdot \delta\left\langle r_\mathrm{c}^2\right\rangle^{60,A}, \qquad (1)$$

with $\mu = (m_A - m_{60})/(m_A \cdot m_{60})$ and $m_A$ being the respective atomic masses. A King-fit analysis was performed using the procedure described in [18] and based on the known rms charge radii of the stable nickel isotopes extracted from the combined analysis of muonic atom data and elastic electron scattering provided in [19]. An $x$-axis offset of $\alpha = 397\,\mathrm{u\,fm^2}$ was used to remove the correlation between $M$ and $F$ and the result of the fit is depicted in Fig. 2. The intercept of the line with the new $y$-axis provides $M_{\alpha=397} = 949(4)\,\mathrm{GHz\,u}$ [corresponding to a mass shift parameter of $M = 1262(32)\,\mathrm{GHz\,u}$] and a field
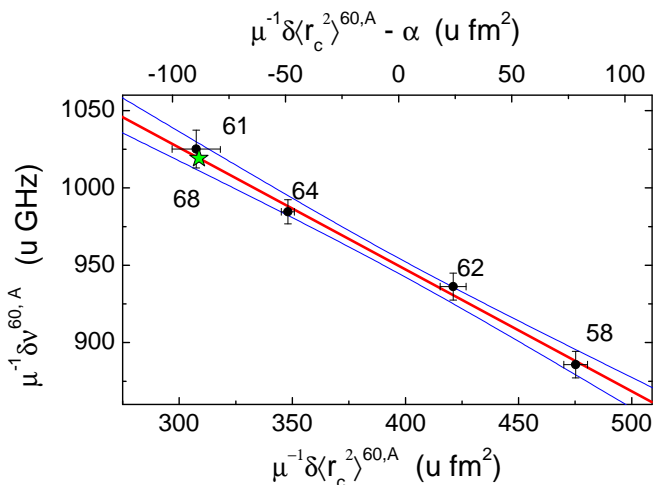
FIG. 2. King-plot analysis of the stable isotopes. The red line is a straight line fit to the black data points taking $x$- and $y$-errors into account and the $1\sigma$-confidence interval is shown as a blue solid line. The top axis is shifted by $\alpha = 397\,\mathrm{u\,fm^2}$ to remove the correlation between $F$ and $M$. The green star shows the position of $^{68}$Ni, from which the charge radius is extracted.

shift parameter of $F = -788(82)\,\mathrm{MHz/fm^2}$. The isotope shift of $^{68}$Ni puts it on the line at the position indicated by a star and the change in the ms charge radius can be calculated with respect to $^{60}$Ni according to

$$\mu^{-1}\,\delta\left\langle r_{\mathrm c}^2\right\rangle^{60,A} = \left(\mu^{-1}\,\delta\nu^{60,A} - M_\alpha\right)/F + \alpha. \quad (2)$$

The results are listed in Table I. With the rms charge radius of $R_{\mathrm c}(^{60}\mathrm{Ni}) = 3.806(2)\,\mathrm{fm}$ taken from [19], the charge radius of $^{68}$Ni is obtained as $R_{\mathrm c}(^{68}\mathrm{Ni}) = 3.887(3)\,\mathrm{fm}$.

TABLE I. Measured isotope shifts $\delta\nu^{60,A}$ relative to $^{60}$Ni with statistical uncertainties in parentheses and systematic uncertainties in square brackets. The statistical uncertainty includes variations between the two beamtimes that are partially of systematic but uncorrelated origin and change statistically from isotope to isotope, while the systematic uncertainty is restricted to the correlated uncertainty caused by the high-voltage measurement. The extracted change in ms charge radius $\delta\left\langle r_c^2\right\rangle^{60,A}$ and the total charge radii $R_{\mathrm c}$ are listed with the total uncertainties.

| $A$ | $\delta\nu^{60,A}$/MHz | $\delta\left\langle r_c^2\right\rangle^{60,A}$/fm$^2$ | $R_{\mathrm c}$/fm |
|---|---|---|---|
| 58 | $-509.1(25)[42]$ | $-0.275(7)$ | 3.770(2) |
| 60 | 0.0 | 0.0 | 3.806(2) |
| 61 | 280.8(27)[20] | 0.083(5) | 3.817(2) |
| 62 | 503.9(25)[39] | 0.223(5) | 3.835(2) |
| 64 | 1027.2(25)[77] | 0.368(9) | 3.854(2) |
| 68 | 1992.3(27)[147] | 0.620(21) | 3.887(3) |

## DISCUSSION

The extracted $R_c$ can be used to benchmark theoretical calculations, to test and expand their reliability and predictive power away from stable nuclei. First principle calculations were recently performed for $^{48}$Ca [8], which lead to an improved understanding of the neutron and proton distributions in nuclei, as well as their difference encoded in $R_{\mathrm{skin}}$. The observed correlation between the dipole polarizability $\alpha_{\mathrm D}$ and the rms charge radius of $^{48}$Ca allowed to narrow down constraints on the dipole polarizability, $\alpha_{\mathrm D} = 2.19 - 2.60\,\mathrm{fm^3}$, and on the neutron skin, $R_{\mathrm{skin}} = 0.12 - 0.15\,\mathrm{fm}$. The latter was found to be considerably smaller than previously thought [8]. The recent Darmstadt-Osaka experimental determination of the dipole polarizability $\alpha_{\mathrm D} = 2.07(22)\,\mathrm{fm^3}$ [5] is indeed in good agreement with the theoretical predictions. Subsequently, new calculations have included higher-order coupled-cluster correlations [20], so-called linearized 3 particles–3 holes ($3p$–$3h$) correlations. This leads to a reduction of the dipole polarizability and to an improved agreement with the experimental data for $^{48}$Ca, while the charge radius is found to not depend sensitively on $3p$–$3h$ correlations [21].

Coupled-cluster calculations of $\alpha_{\mathrm D}$ based on chiral EFT interactions, initiated in Refs. [8, 20–24], have progressed towards heavier, more complex nuclei and have now reached the short-lived $^{68}$Ni. Contrary to the stable isotopes, for which inelastic proton scattering was used to experimentally access the dipole polarizability, $\alpha_{\mathrm D}$ of $^{68}$Ni was determined using Coulomb excitation in inverse kinematics by measuring the invariant mass in the one- and two-neutron decay channels [12]. This result, subsequently refined in Ref. [25], is shown together with our first experimental determination of $R_{\mathrm c}$ in Fig. 3. Figure 3 also shows our theoretical results using four different chiral nucleon-nucleon (NN) and three-nucleon (3N) interactions from Ref. [26] (with the same labeling used here: 1.8/2.0, 2.0/2.0, 2.2/2.0 (EM) and 2.0/2.0 (PWA)) as well as the NNLO$_{\mathrm{sat}}$ interaction from Ref. [27]. The Hamiltonians of Ref. [26] are based on a chiral N$^3$LO NN potential evolved to low resolution using the similarity renormalization group combined with N$^2$LO 3N interactions fit to the $^3$H binding energy and the $^4$He charge radius. These interactions have been successfully used to study the structure of medium-mass nuclei up to $^{100}$Sn (see, e.g., Refs. [28–31]).

Figure 3 shows two sets of coupled-cluster calculations: one with singles and doubles correlations (dashed points, line and light blue band) and another one where the leading $3p$–$3h$ correlations are included (solid points and line with darker blue band). We observe that triples corrections lead to a sizable reduction of $\alpha_{\mathrm D}$ (from 8% for the softest NN+3N interactions 1.8/2.0 (EM) to 15% for the hardest NNLO$_{\mathrm{sat}}$ interaction), while $R_c$ is changed
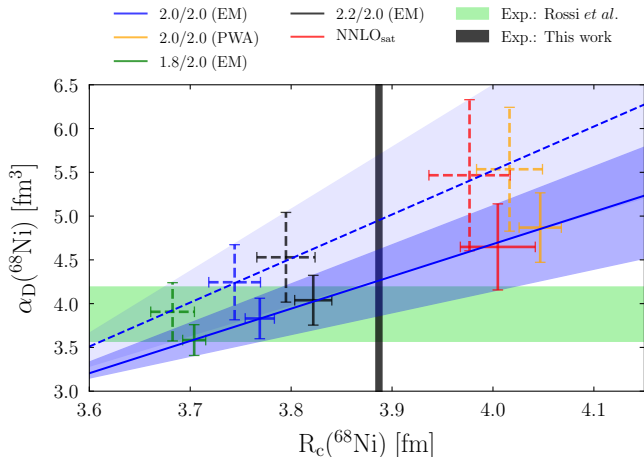
FIG. 3. Theoretical results for the rms charge radius $R_c$ and the dipole polarizability $\alpha_D$ of $^{68}$Ni in comparison with experiment. The horizontal bar represents $\alpha_D$ measured by Rossi *et al.* [12] and refined by Roca-Maza *et al.* [25] to $\alpha_D = 3.88(31)\,\text{fm}^3$. The vertical bar represents the rms charge radius $R_c = 3.887(3)\,\text{fm}$ determined in this work. The blue lines and bands are fits to the theoretical results for the different chiral NN and 3N interactions (crosses, see text for details) based on the coupled-cluster calculations with singles and doubles excitations (dashed line and light blue band) and when $3p$–$3h$ correlations are included (solid line and darker blue band). The widths of the bands are chosen to include the full error bars of the individual calculations.

only mildly (maximally 0.7% for the hardest interaction). Each theoretical point is shown with a corresponding estimate of the theoretical uncertainty, which includes both the residual model-space dependence and the coupled-cluster truncation error, following the protocol explained in Ref. [21]. As expected, the uncertainties are smaller (larger) for soft (hard) interactions. For completeness, the charge radius $R_c$ is obtained from the point-proton radius $R_p$ by

$$R_c^2 = R_p^2 + \langle r_p^2 \rangle + (N/Z)\langle r_n^2 \rangle + (3/4M^2) + \langle r^2 \rangle_{\text{so}}, \quad (3)$$

where $\langle r_p^2 \rangle = 0.7080(32)\,\text{fm}^2$ [32] and $\langle r_n^2 \rangle = -0.117(4)\,\text{fm}^2$ [33] are the rms charge radii of a proton and a neutron, respectively, $(3/4M^2) = 0.033\,\text{fm}^2$ [34] is the relativistic Darwin-Foldy correction and $\langle r^2 \rangle_{\text{so}}$ is the spin-orbit correction for $^{68}$Ni, which we calculate consistently for each Hamiltonian.

It is interesting to note that the behavior is very similar to that observed for the stable nucleus $^{48}$Ca [5, 8, 20, 21]. The theoretical results exhibit a clear correlation between the dipole polarizability and the charge radius both at the singles-and-doubles and triples excitations level. The inclusion of triples excitations, however, alters the slope of this correlation. In Fig. 3, the correlation is highlighted by the linear fit to the calculations and the corresponding blue uncertainty bands, which are chosen to include

the full error bars of the individual calculations. Most notably, for the results with singles and doubles excitations, the band does not overlap with the intersection region of the measured $R_c$ and $\alpha_D$. When including $3p$–$3h$ correlations, the theoretical band nicely overlaps with the experimental constraints. This shows that $3p$–$3h$ correlations are not negligible, and that state-of-the-art coupled-cluster computations are reliable for this first test of the charge radius and $\alpha_D$ of the neutron-rich nucleus $^{68}$Ni.

Compared to the results $\alpha_D = 3.60\,\text{fm}^3$ obtained recently by Raimondi and Barbieri [35] with the self-consistent Green's function method using the NNLO$_{\text{sat}}$ interaction, we obtain a considerably larger value of $\alpha_D = 4.65(49)\,\text{fm}^3$ using the same interaction. The reason of the discrepancy could either be due to the different method used, or more likely related to the larger $\hbar\Omega$ value in Ref. [35]. The central value of our coupled-cluster results are obtained with $\hbar\Omega = 12\,\text{MeV}$, which shows a very nice convergence pattern as a function of the model-space size; while we have observed that larger $\hbar\Omega$ values exhibit a much slower convergence.

In addition to our ab initio calculations, the dipole polarizability of $^{68}$Ni was also studied with nuclear EDFs, which suggested that $\alpha_D$ is strongly correlated with the neutron skin and this correlation is even stronger when information on the symmetry energy is taken into account [25]. This led to a prediction of the neutron skin $R_{\text{skin}} = 0.16(4)\,\text{fm}$ [25] of $^{68}$Ni. In Table II we list the coupled-cluster results including $3p$–$3h$ corrections for the optimal $\hbar\Omega$ for the different chiral NN and 3N interactions studied. Taking as best interactions for the correlation plot, Fig. 3, the ones closest to the intersection region, 2.0/2.0 (EM), 2.2/2.0 (EM), and NNLO$_{\text{sat}}$, we predict in Table II a range for the point-neutron radius $R_n = 3.9 - 4.1\,\text{fm}$ of $^{68}$Ni and its neutron skin $R_{\text{skin}} = 0.18 - 0.20\,\text{fm}$, in very good agreement with the EDF correlation prediction of Ref. [25].

## SUMMARY

We have presented the first measurement of the isotope shift of the neutron-rich $^{68}$Ni isotope by collinear laser spectroscopy. This enabled the extraction of the rms charge radius to $R_c = 3.887(3)\,\text{fm}$ based on a King-plot analysis and the known charge radii of the stable nickel isotopes. This radius is used to benchmark coupled-cluster calculations including novel triples corrections for a range of chiral NN and 3N interactions. A strong correlation between the charge radius and the dipole polarizability is shown by the theoretical calculations. Our results including the leading $3p$–$3h$ contributions agree much better with the experimental data compared to the case when triples corrections are neglected. In particular the theoretical correlation band intersects nicely with the measured $R_c$ and $\alpha_D$ bands.

TABLE II. Coupled-cluster results including $3p$–$3h$ corrections for $\alpha_{\rm D}$ in fm$^3$ and $R_{\rm p}$, $R_{\rm n}$, $R_{\rm skin}$, $R_{\rm c}$ in fm for $^{68}$Ni for the different chiral NN and 3N interactions studied [26, 27]. The central values are for the optimal harmonic-oscillator frequency $\hbar\Omega = 12$ MeV.

| Hamiltonian | $\alpha_{\rm D}$ | $R_{\rm p}$ | $R_{\rm n}$ | $R_{\rm skin}$ | $R_{\rm c}$ |
|---|---|---|---|---|---|
| 1.8/2.0 (EM) | 3.58(18) | 3.62(1) | 3.82(1) | 0.201(1) | 3.70(1) |
| 2.0/2.0 (EM) | 3.83(23) | 3.69(2) | 3.89(2) | 0.202(3) | 3.77(1) |
| 2.2/2.0 (EM) | 4.04(28) | 3.74(2) | 3.94(2) | 0.203(4) | 3.82(2) |
| 2.0/2.0 (PWA) | 4.87(40) | 3.97(2) | 4.17(3) | 0.204(8) | 4.05(2) |
| NNLO$_{\rm sat}$ | 4.65(49) | 3.93(4) | 4.11(5) | 0.183(8) | 4.00(4) |

This correlation combined with coupled-cluster calculations of the point-neutron radius and neutron skin of $^{68}$Ni allows these to be constrained to $R_n = 3.9 - 4.1$ fm and $R_{\rm skin} = 0.18 - 0.20$ fm.

$^*$ wnoertershaeuser@ikp.tu-darmstadt.de

[1] B. P. Abbott, R. Abbott, T. D. Abbott, F. Acernese, K. Ackley, C. Adams, T. Adams, P. Addesso, R. X. Adhikari, V. B. Adya, et al. (The LIGO Scientific Collaboration and the Virgo Collaboration), Phys. Rev. Lett. **121**, 161101 (2018).

[2] P. Danielewicz, R. Lacey, and W. G. Lynch, Science **298**, 1592 (2002).

[3] M. B. Tsang, J. R. Stone, F. Camera, P. Danielewicz, S. Gandolfi, K. Hebeler, C. J. Horowitz, J. Lee, W. G. Lynch, Z. Kohley, et al., Phys. Rev. C **86**, 015803 (2012).

[4] X. Roca-Maza, M. Centelles, X. Viñas, and M. Warda, Phys. Rev. Lett. **106**, 252501 (2011).

[5] J. Birkhan, M. Miorelli, S. Bacca, S. Bassauer, C. A. Bertulani, G. Hagen, H. Matsubara, P. von Neumann-Cosel, T. Papenbrock, N. Pietralla, et al., Phys. Rev. Lett. **118**, 252501 (2017).

[6] T. Hashimoto, A. M. Krumbholz, P.-G. Reinhard, A. Tamii, P. von Neumann-Cosel, T. Adachi, N. Aoi, C. A. Bertulani, H. Fujita, Y. Fujita, et al., Phys. Rev. C **92**, 031305(R) (2015).

[7] A. Tamii, I. Poltoratska, P. von Neumann-Cosel, Y. Fujita, T. Adachi, C. A. Bertulani, J. Carter, M. Dozono, H. Fujita, K. Fujita, et al., Phys. Rev. Lett. **107**, 062502 (2011).

[8] G. Hagen, A. Ekström, C. Forssén, G. R. Jansen, W. Nazarewicz, T. Papenbrock, K. A. Wendt, S. Bacca, N. Barnea, B. Carlsson, et al., Nat. Phys. **12**, 186 (2015).

[9] E. Epelbaum, H.-W. Hammer, and U.-G. Meißner, Rev. Mod. Phys. **81**, 1773 (2009).

[10] R. Machleidt and D. Entem, Phys. Rep. **503**, 1 (2011).

[11] H.-W. Hammer, A. Nogga, and A. Schwenk, Rev. Mod. Phys. **85**, 197 (2013).

[12] D. M. Rossi, P. Adrich, F. Aksouh, H. Alvarez-Pol, T. Aumann, J. Benlliure, M. Böhmer, K. Boretzky, E. Casarejos, M. Chartier, et al., Phys. Rev. Lett. **111**, 242503 (2013).

[13] B. A. Marsh, Rev. Sci. Instrum. **85**, 02B923 (2014).

[14] H. Frånberg, P. Delahaye, J. Billowes, K. Blaum, R. Catherall, F. Duval, O. Gianfrancesco, T. Giles, A. Jokinen, M. Lindroos, et al., Nucl. Instr. Meth. Phys. Res. B **266**, 4502 (2008).

[15] A. Mueller, F. Buchinger, W. Klempt, E. Otten, R. Neugart, C. Ekström, and J. Heinemeier, Nucl. Phys. A **403**, 234 (1983).

[16] A. Klose, K. Minamisono, C. Geppert, N. Frömmgen, M. Hammen, J. Krämer, A. Krieger, C. Levy, P. Mantica, W. Nörtershäuser, et al., Nucl. Instr. Meth. Phys. Res. A **678**, 114 (2012).

[17] C. Ryder, K. Minamisono, H. Asberry, B. Isherwood, P. Mantica, A. Miller, D. Rossi, and R. Strum, Spectroch. Acta B **113**, 16 (2015).

[18] M. Hammen, W. Nörtershäuser, D. L. Balabanski, M. L. Bissell, K. Blaum, I. Budinčević, B. Cheal, K. T. Flanagan, N. Frömmgen, G. Georgiev, et al., Phys. Rev. Lett. **121**, 102501 (2018).

[19] G. Fricke and K. Heilig, Nuclear Charge Radii, Group I: Elementary Particles, Nuclei and Atoms, Vol. 20 (Springer, 2004).

[20] M. Miorelli, S. Bacca, G. Hagen, and T. Papenbrock, Phys. Rev. C **98**, 014324 (2018).

[21] J. Simonis, S. Bacca, and G. Hagen, Eur. Phys. J. A **55**, 241 (2019).

[22] S. Bacca, N. Barnea, G. Hagen, G. Orlandini, and T. Papenbrock, Phys. Rev. Lett. **111**, 122502 (2013).

[23] S. Bacca, N. Barnea, G. Hagen, M. Miorelli, G. Orlandini, and T. Papenbrock, Phys. Rev. C **90**, 064619 (2014).

[24] M. Miorelli, S. Bacca, N. Barnea, G. Hagen, G. R. Jansen, G. Orlandini, and T. Papenbrock, Phys. Rev. C **94**, 034317 (2016).

[25] X. Roca-Maza, X. Viñas, M. Centelles, B. K. Agrawal, G. Colò, N. Paar, J. Piekarewicz, and D. Vretenar, Phys. Rev. C **92**, 064304 (2015).

[26] K. Hebeler, S. K. Bogner, R. J. Furnstahl, A. Nogga, and A. Schwenk, Phys. Rev. C **83**, 031301(R) (2011).

[27] A. Ekström, G. R. Jansen, K. A. Wendt, G. Hagen, T. Papenbrock, B. D. Carlsson, C. Forssén, M. Hjorth-Jensen, P. Navrátil, and W. Nazarewicz, Phys. Rev. C **91**, 051301(R) (2015).

[28] J. Simonis, K. Hebeler, J. D. Holt, J. Menéndez, and A. Schwenk, Phys. Rev. C **93**, 011302(R) (2016).

[29] J. Simonis, S. R. Stroberg, K. Hebeler, J. D. Holt, and A. Schwenk, Phys. Rev. C **96**, 014303 (2017).

[30] T. D. Morris, J. Simonis, S. R. Stroberg, C. Stumpf, G. Hagen, J. D. Holt, G. R. Jansen, T. Papenbrock, R. Roth, and A. Schwenk, Phys. Rev. Lett. **120**, 152503 (2018).

[31] J. D. Holt, S. R. Stroberg, A. Schwenk, and J. Simonis, (2019), arXiv:1905.10475.

[32] `https://physics.nist.gov/cgi-bin/cuu/Value?rp` (2019).

[33] S. Kopecky, J. A. Harvey, N. W. Hill, M. Krenn, M. Pernicka, P. Riehs, and S. Steiner, Phys. Rev. C **56**, 2229 (1997).

[34] J. L. Friar, J. Martorell, and D. W. L. Sprung, Phys. Rev. A **56**, 4579 (1997).

[35] F. Raimondi and C. Barbieri, Phys. Rev. C **99**, 054327 (2019).